BALKAN JOURNAL OF ELECTRICAL & COMPUTER ENGINEERING, Vol. 13, No. 4, December 2025
Research Article

Hardware-Based Simulator for Hydrodynamic Pitch and Roll Behavior of Marine Vehicles

Ufuk Guner

***Abstract*—This study presents the design of a hardware-based simulator to examine the impact of sea waves on ship navigation sensors. The objective is to create a cost-efficient, easily deployable, and effective simulator. The study considers the pitch and roll movements arising from the wave-heave relationship. A simulator comprising a single rotary actuator is built for this purpose. The mathematical model characterizing the ship-wave interaction is employed to obtain the motion profile. A sequence control with a real-time control parameter update algorithm is developed to track the motion profile. The simulator's performance is validated through experimental studies. The simulator demonstrates a tracking error of less than 0.012 radians. The simulator may also utilize motion profiles established via various wave-ship models. The compact dimensions of the simulator facilitate on-site testing and analysis.**

***Index Terms*—Hardware-in-the-loop, rotation simulator, motion profile control, sequence controller**

I. Introduction

RELIABLE ship navigation systems are essential for safety, efficiency, and automation. To provide accurate performance in current navigation systems, sensors such as GNSS, IMU, and radar must work with great precision. IMU sensors, in particular, play an important role in delivering crucial acceleration and angular rate measurements, which are required for navigation and to compensate dynamic motions in severe maritime settings. However, wave and wind-induced disturbances can lead to inaccuracies in sensor data and system integration issues. The large size of marine vessels and the high operational costs make it difficult to test real-time developments of navigation sensors. Therefore, testing with hardware-in-the-loop (HIL) simulation systems, which integrate real hardware components into a controlled test environment, offers significant advantages for problem detection and system performance validation [1].

In experimental studies on ship navigation and control, wave-generating pools, Stewart platforms, and multi-axis turntables can be used as simulators. Considering the difficulty and cost of real sea trials, simulators provide a significant advantage.

A Stewart platform controlled by a neural network trained with motion data obtained from real sea trials is used to simulate yacht movements [2]. The system accurately reproduces yacht movements, providing a practical and cost-effective solution for ship navigation simulators, with accuracies of the roll and pitch movements of 0.0354 and 0.0270 radians, respectively. In another study, a method was proposed to eliminate the effects of roll and pitch rotation on heave measurement to enhance the efficiency of ship motion control [3]. Different ship motion scenarios were simulated using a 3-DoF rotary table built in a laboratory environment for validation. In [4], a sensor fusion and height-prediction adaptive filtering method for the active heave compensation approach is proposed, and the experiments require a massive setup capable of simulating marine platforms.

To estimate a ship's mass and center of mass using IMU data, the ship's heave dynamics were modeled as a pendulum [5]. To validate the model's performance, experiments were conducted using a pendulum system constructed with a servo actuator.

In a study on wave measurement using low-cost MEMS accelerometers [6], a 6-DoF Stewart-based platform was used to achieve directional wave measurement performance. Talke et al. employed a 3-DoF, low-cost prismatic-spherical-revolute parallel mechanism and an IMU to simulate boat motion. They stated that the motion error margin is less than 2° [7]. H. Yongpan et al. proposed a method to enhance the accuracy of heave measurements using real-time zero-phase filtering with successive high-pass filters [8], and a Stewart-based parallel motion simulator is used to generate the heave motion. In [9], a 6-DoF Stewart-like motion platform is used to evaluate an isolation system designed to protect ship navigation accelerometers from noise and vibration. X. Lui et al. proposed a method for shortening transfer alignment and increasing accuracy in inertial navigation systems. Experimental verification was carried out using a precision turntable [10].

Stewart-like motion platforms offer significant advantages for simulating wave and ship behaviors. Providing movement in linear coordinates, in particular, ensures realistic experimental results. However, Stewart-like motion platforms are nonlinear in their mechanical design and motion behavior. Therefore, it is necessary to reduce simulator-induced errors. This requires complex modeling and controller structures, resulting in the need for a highly precise mechanical design. The turntables are high-precision test and calibration systems that can produce precise rotational motion. However, increasing the number of rotational axes requires precise and bulky mechanical structures.

In studies conducted close to real-world systems, open sea environments or wave-generating pools can be used. In a study, a pool area is used for validation experiments of a calibration method addressing rotation and displacement errors in mobile measurement systems on ships [11]. Another study aimed at developing a computer control system for an

Ufuk GÜNER, are with the Department of Electrical and Electronics Engineering, Erzurum Technical University, Erzurum, 25050, TURKEY, e-mails: ufuk.guner@erzurum.edu.tr
Manuscript received Mar 19, 2025; accepted Jun 10, 2025.
DOI: 10.17694/bajece.1661442

unmanned ship model equipped with sensors and navigation devices [12]. Experimental studies were conducted at sea with an unmanned autonomous ship model. Y. Ma et al. introduced an accurate measurement method for the heave motion using Kalman filtering and traditional high-pass filters, which included a sliding adaptive delayless complementary band-pass algorithmic filter [13]. To evaluate the effectiveness of the algorithm, experimental studies were conducted in a real sea environment. L. Wang et al. investigated the integration of a smart optimization controller with a traditional controller to improve ship navigation.Motion states and navigation scenarios were simulated in an open pool environment with a prototype model ship [14].

The biggest limitation in studies carried out in marine and open pool environments is that suitable conditions can not be maintained permanently. Moreover, wave-generating pools are not accessible as experimental environments for every researcher.

The studies summarized above comprehensively highlight both the importance and the advantages offered by hardware-based simulator systems developed for the calibration of sensors and the validation of filtering algorithms in ship navigation systems. These systems provide significant benefits such as early error detection, high repeatability, and cost-effectiveness through real hardware integration, while also having disadvantages such as modeling errors, high costs, and limited accessibility.

This research proposes a hardware-based wave simulator for inertial sensors. The proposed simulator allows for the analysis of sensor systems dependent on the wave-ship interaction. Here is a list of the study's primary contributions:

- The proposed simulator is cost-effective. It includes only one actuator with an absolute encoder.
- A novel sequence controller is proposed. The controller allows point-by-point tracking of a trajectory.
- The control architecture is easy to implement. It can realize motion profiles obtained from real-time data or simulation data.
- The simulator consists of a single actuator, which reduces mechanical complexity and mechanical errors.
- The simulator is portable, it can be configured for on-site testing and analysis.

The proposed simulator has a simple architecture. It uses a model reflecting the sea-wave interaction. The model provides a motion profile. A brushless DC motor is used to transfer the motion profile to the tested system. An absolute encoder is used for feedback. The motion profile is tracked by a sequence controller.The sequence controller is cascade-structured. The target step is controlled by an internal PI controller located in the sequence controller. The internal controller operates at high frequencies. The tracking performance is enhanced by an algorithm that updates parameters of the internal PI controller automatically to reach target steps on time. The The simulator provides a useful experimental environment for testing and analyzing sensors used in roll and pitch measurements.

II. Motion Model for Marine Vehicles

The hardware-based simulator requires the marine vehicle's motion profile.Therefore, a motion model that represents sea behavior is required. In this study, the basic motion model is used as a reference. When marine vehicles are considered as rigid bodies, they can be modeled with six-degrees-of-freedom equations of motion. The motion of the vehicle in linear coordinates is expressed by x, y, and z. Additionally, the vehicle has roll, pitch, and yaw rotations. This study aims to develop a hardware-based simulator for wave-induced pitch and roll motion. The pitch and roll motions of the marine vehicles are induced by waves. Waves cause the marine vehicle to rise and rotate. As a results, the rigid body of the marine vehicle responds with linear motion along the z axis and rotational motion around the x and y axes. Fig. 1 shows the coordinates and rotation variables of a marine vehicle.

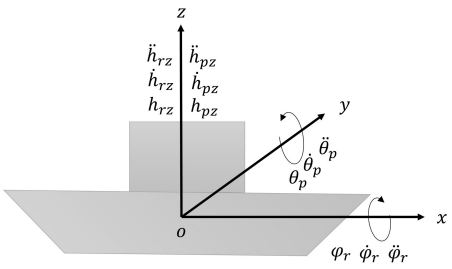

Fig. 1: Coordinate of marine vehicle

θ_p, $\dot{\theta}_p$, and $\ddot{\theta}_p$ are respectively the position, velocity, and acceleration of the pitch motion. The position, velocity, and acceleration of the roll motion are represented by φ_r, $\dot{\varphi}_p$, and $\ddot{\varphi}_r$, respectively. Heave moves the vehicle up and down along the z-axis. This situation may occur together with roll or pitch movements. The motion on the z-axis that occurs with the pitch motion is modeled by h_{pz}, $\dot{h}_{pz}$, $\ddot{h}_{pz}$. The motion on the z axis that occurs with the roll motion is modeled by h_{rz}, $\dot{h}_{rz}$, $\ddot{h}_{rz}$. In this study, the simulator has single actuator, thus a discrete modeling is applied for roll and pitch. Considering coupled effect between pitch and heave [15], [16], the equation of pitch motion is defined as

$$\begin{aligned}&(m_s + m_{33})\,\ddot{h}_{pz} + d_{33}\dot{h}_{pz} + c_{33}h_{pz} + \\ &m_{35}\ddot{\theta}_p + d_{35}\dot{\theta}_p + c_{35}\theta_p = F_p(t) \\ &(I_p + I_{55})\,\ddot{\theta}_p + d_{55}\dot{\theta}_p + c_{55}\theta_p + \\ &m_{53}\ddot{h}_{pz} + d_{53}\dot{h}_{pz} + c_{53}h_{pz} = P_p(t).\end{aligned} \tag{1}$$

A similar situation is valid for the roll motion. The equation of roll motion can be defined as

$$\begin{aligned}&(m_s + m_{33})\,\ddot{h}_{rz} + d_{33}\dot{h}_{rz} + c_{33}h_{rz} + \\ &m_{34}\ddot{\varphi}_r + d_{34}\dot{\varphi}_r + c_{34}\varphi_r = F_r(t) \\ &(I_r + I_{44})\,\ddot{\varphi}_r + d_{44}\dot{\varphi}_r + c_{44}\varphi_r + \\ &m_{43}\ddot{h}_{rz} + d_{43}\dot{h}_{rz} + c_{43}h_{rz} = P_r(t).\end{aligned} \tag{2}$$

The coupled heave–pitch and heave–roll equations define the inertia, damping, and stiffness of each degree of freedom under wave excitation through cross-coupling. The ship's rigid mass m_s and inertia I_p, I_r are defined by the hydrodynamic added

mass coefficients m_{33} that is the additional mass caused by the acceleration of the body, which also accelerates some of the surrounding fluids. This also causes additional inertia (I_{44},I_{55}). Damping coefficients d_{ii} model the energy lost to the waves being propagated. Hydrostatic restoring stiffnesses c_{ii} arise from buoyancy and trim moments. Cross terms, such as m_{ij}, d_{ij}, c_{ji} and their counterparts, define how vertical and rotational motions interact when the center of buoyancy and center of gravity are misaligned. External wave excitation forces and moments are defined as $F_{p,r}(t)$ and $P_{p,r}(t)$, respectively. General definition of the parameters are listed in Table I.

TABLE I: Definitions of the parameters

Coefficients	Definition
m_s	Ship mass
I_p,I_r	Moment of inertia
m_{ii},m_{ij}	Added mass
I_{55}, I_{44}	Added inertia
d_{ii},d_{ij}	Heave damping (effect of water resistance)
c_{ii},c_{ij}	Elastic coefficients (return to equilibrium)
$F_p(t)$,$F_r(t)$	Heave external force for pitch and roll
$P_p(t)$,$P_r(t)$	Pitch and roll external moment

As can be seen in (1) and (2), the only difference between the roll and pitch equations is in their terms. Therefore, to avoid repetition, only the derivation of the pitch motion is presented. The roll state-space model is presented directly. The pitch motion states are defined as

$$x_p = [h_{pz} \quad \dot{h}_{pz} \quad \theta_p \quad \dot{\theta}_p]^T$$

and, the state space form of pitch motion is

$$M_p \dot{x}_p = A x_p + B u_p \tag{3}$$

where M_p is mass matrix and $u_p = [F_p \quad P_p]^T$. It is assumed that M_p is invertible, the state space model can be rearrange as

$$\dot{x}_p = \underbrace{M_p^{-1} A}_{A_p} x_p + \underbrace{M_p^{-1} B}_{B_p} u_p \tag{4}$$

Rewriting in matrix form to solve for $\ddot{h}_{pz}$ and $\ddot{\theta}_p$

$$\begin{bmatrix} m_s + m_{33} & m_{35} \\ m_{53} & I_p + I_{55} \end{bmatrix} \begin{bmatrix} \ddot{h}_{pz} \\ \ddot{\theta}_p \end{bmatrix} = \begin{bmatrix} -d_{33}\dot{h}_{pz} - d_{35}\dot{\theta}_p - c_{33}h_{pz} - c_{35}\theta_p + F_p \\ -d_{53}\dot{h}_{pz} - d_{55}\dot{\theta}_p - c_{53}h_{pz} - c_{55}\theta_p + P_p \end{bmatrix} \tag{5}$$

and inverting the mass matrix

$$M_{\mathrm{p}}^{-1} = \frac{1}{\Delta_p} \begin{bmatrix} I_p + I_{55} & -m_{35} \\ -m_{53} & m_s + m_{33} \end{bmatrix}, \quad \Delta_p = (m_s + m_{33})(I_p + I_{55}) - m_{35}m_{53}. \tag{6}$$

So, $\ddot{h}_{pz}$ and $\ddot{\theta}_p$ can be rearranged as

$$\begin{bmatrix} \ddot{h}_{pz} \\ \ddot{\theta}_p \end{bmatrix} = -M_{\mathrm{p}}^{-1} \begin{bmatrix} d_{33} & d_{35} \\ d_{53} & d_{55} \end{bmatrix} \begin{bmatrix} \dot{h}_{pz} \\ \dot{\theta}_p \end{bmatrix} - M_{\mathrm{p}}^{-1} \begin{bmatrix} c_{33} & c_{35} \\ c_{53} & c_{55} \end{bmatrix} \begin{bmatrix} h_{pz} \\ \theta_p \end{bmatrix} + M_{\mathrm{p}}^{-1} \begin{bmatrix} F_p \\ P_p \end{bmatrix}. \tag{7}$$

Thus, the state transition and input matrix can be obtained as

$$A_p = \begin{bmatrix} 0 & 1 & 0 & 0 \\ \frac{-M_{p22}c_{33}+m_{35}c_{53}}{\Delta_p} & \frac{-M_{p22}d_{33}+m_{35}d_{53}}{\Delta_p} & \frac{-M_{p22}c_{35}+m_{35}c_{55}}{\Delta_p} & \frac{-M_{p22}d_{35}+m_{35}d_{55}}{\Delta_p} \\ 0 & 0 & 0 & 1 \\ \frac{m_{53}c_{33}-M_{p11}c_{53}}{\Delta_p} & \frac{m_{53}d_{33}-M_{p11}d_{53}}{\Delta_p} & \frac{m_{53}c_{35}-M_{p11}c_{55}}{\Delta_p} & \frac{m_{53}d_{35}-M_{p11}d_{55}}{\Delta_p} \end{bmatrix} \tag{8}$$

$$B_p = \begin{bmatrix} 0 & 0 \\ \frac{M_{p22}}{\Delta_p} & \frac{-m_{35}}{\Delta_p} \\ 0 & 0 \\ \frac{-m_{53}}{\Delta_p} & \frac{M_{p11}}{\Delta_p} \end{bmatrix} \tag{9}$$

where

$$M_{p11} = m_s + m_{33}$$
$$M_{p22} = I_p + I_{55}.$$

The state space form of roll motion can be defined as

$$\dot{x}_r = \underbrace{M_r^{-1} A}_{A_r} x_r + \underbrace{M_r^{-1} B}_{B_r} u_r \tag{10}$$

where M_r is mass matrix of roll motion and $u_r = [F_r \quad P_r]^T$. The states are defined as follows.

$$x_r = [h_{rz} \quad \dot{h}_{rz} \quad \varphi_r \quad \dot{\varphi}_r]^T$$

M_r is assumed as invertible, and M_{r}^{-1} is defined as

$$M_{\mathrm{r}}^{-1} = \frac{1}{\Delta_r} \begin{bmatrix} I_r + I_{44} & -m_{34} \\ -m_{43} & m_s + m_{33} \end{bmatrix}, \quad \Delta_r = (m_s + m_{33})(I_r + I_{44}) - m_{43}m_{34}. \tag{11}$$

For roll motion model, the state transition and input matrix can be obtained as

$$A_r = \begin{bmatrix} 0 & 1 & 0 & 0 \\ \frac{-M_{r22}c_{33}+m_{34}c_{43}}{\Delta_r} & \frac{-M_{r22}d_{33}+m_{34}d_{43}}{\Delta_r} & \frac{-M_{r22}c_{34}+m_{34}c_{44}}{\Delta_r} & \frac{-M_{r22}d_{34}+m_{34}d_{44}}{\Delta_r} \\ 0 & 0 & 0 & 1 \\ \frac{m_{43}c_{33}-M_{r11}c_{43}}{\Delta_r} & \frac{m_{43}d_{33}-M_{r11}d_{43}}{\Delta_r} & \frac{m_{43}c_{34}-M_{r11}c_{44}}{\Delta_r} & \frac{m_{43}d_{34}-M_{r11}d_{44}}{\Delta_r} \end{bmatrix} \tag{12}$$

$$B_r = \begin{bmatrix} 0 & 0 \\ \frac{M_{r22}}{\Delta_r} & \frac{-m_{34}}{\Delta_r} \\ 0 & 0 \\ \frac{-m_{43}}{\Delta_r} & \frac{M_{r11}}{\Delta_r} \end{bmatrix} \tag{13}$$

where

$$M_{r11} = m_s + m_{33}$$
$$M_{r22} = I_r + I_{44}.$$

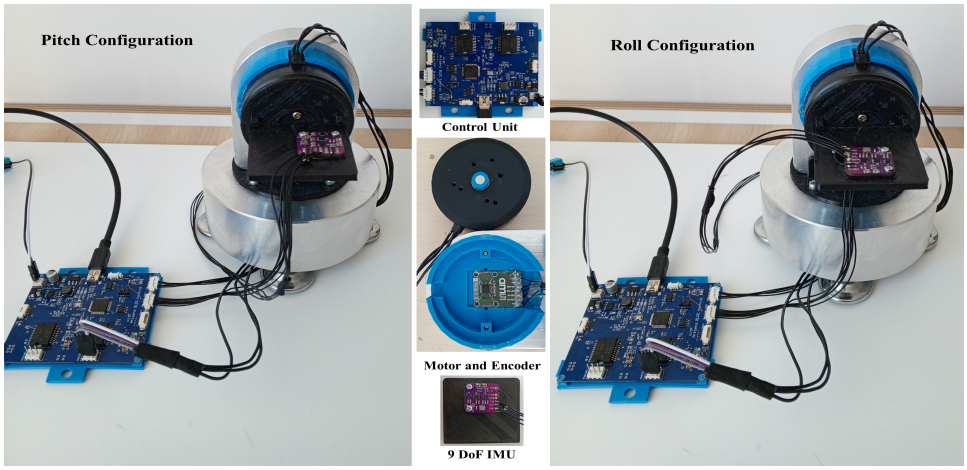

Fig. 2: Pitch and roll configuration of the simulator.

III. Configuration of Simulator

The hardware-based simulator consists of three essential components: a brushless DC motor(GBM5108-120T), an absolute encoder(AS5048A), and a control unit. Fig. 2 shows the structure of the simulator. The motor and encoder are responsible for generating smooth rotation. The control unit drives the motor using feedback from the encoder. The control unit has an STM32F405RB microcontroller with a processing speed of 168 MHz. It includes a single-chip L6234 integrated circuit with three half-bridge circuits to drive the brushless motor. There are two L6234 motor drivers. Only one L6234 is used in this study. The L6234 driver is controlled by microcontroller PWM outputs. The SPI (Serial Peripheral Interface), CAN (Controller Area Network), I2C (Inter-Integrated Circuit), and USB (Universal Serial Bus) interfaces of the processor are accessible in the control unit. The SPI interface is used for communication with the magnetic encoder. The I2C interface is used for communication with the sensor unit. The USB and CAN interfaces are used for data communication with MATLAB. Fig. 3 shows the structure of the controller unit.

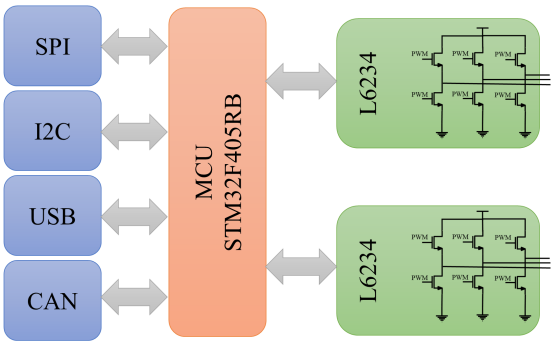

Fig. 3: Structure of the controller unit.

The microcontroller also executes the motion tracking algorithm. The purpose of the hardware-based simulator is the analysis of the navigation system, including an IMU. Therefore, there is a 9-DoF inexpensive IMU connected to the rotor of the motor. It is possible to excite roll and pitch sensors with the changing position of the IMU. The magnetic absolute encoder uses a pole-paired magnet to measure the angular position. The resolution of the encoder is 14 bits. Thus, it can measure position with 0.0439° or 0.0007 rad sensitivity. The brushless motor contains a pole-paired rotor and magnet. Thus, to drive the motor, it needs to know the beginning of the pole pair. With the absolute encoder, it is possible to define the initial pole and control the motor position. The IMU consists of a MAX2100 inertial sensor that includes a three-axis accelerometer and a three-axis gyroscope. It serves only as a test system within the simulator and is not used for control. Additionally, the IMU has two distinct three-axis magnetometer, which are not used in this study.

IV. Motion Profile

The simulator is expected to produce a predefined movement. Therefore, a motion profile is required. The motion profile defines the desired motion over time, specifying position, velocity, acceleration, and sometimes jerk. It ensures smooth, efficient, and physically feasible movement.

TABLE II: Model parameter values

Pitch	Value	Roll	Value
m_s	1.5×10^6 kg	m_s	1.5×10^6 kg
m_{33}	0.7×10^6 kg	m_{33}	0.7×10^6 kg
d_{33}	2×10^6 Ns/m	d_{33}	2×10^6 Ns/m
c_{33}	1×10^7 N/m	c_{33}	1×10^7 N/m
I_p	2×10^9 kgm^2	I_r	2.5×10^9 kgm^2
I_{55}	0.8×10^9 N/m	I_{44}	0.8×10^9 N/m
d_{55}	5×10^7 Nms/rad	d_{44}	5×10^7 Nms/rad
c_{55}	8×10^8 Nm/rad	c_{44}	8×10^8 Nm/rad
m_{35},m_{53}	2×10^5 kgm	m_{34},m_{43}	2×10^5 kgm
d_{35},d_{53}	1×10^6 Ns	d_{34},d_{43}	1×10^6 Ns
c_{35},c_{53}	3×10^6 Nm	c_{34},c_{43}	3×10^6 Nm

In this study, the model that is defined in Section II is used to determine the motion. The sea waves cause heave in a marine

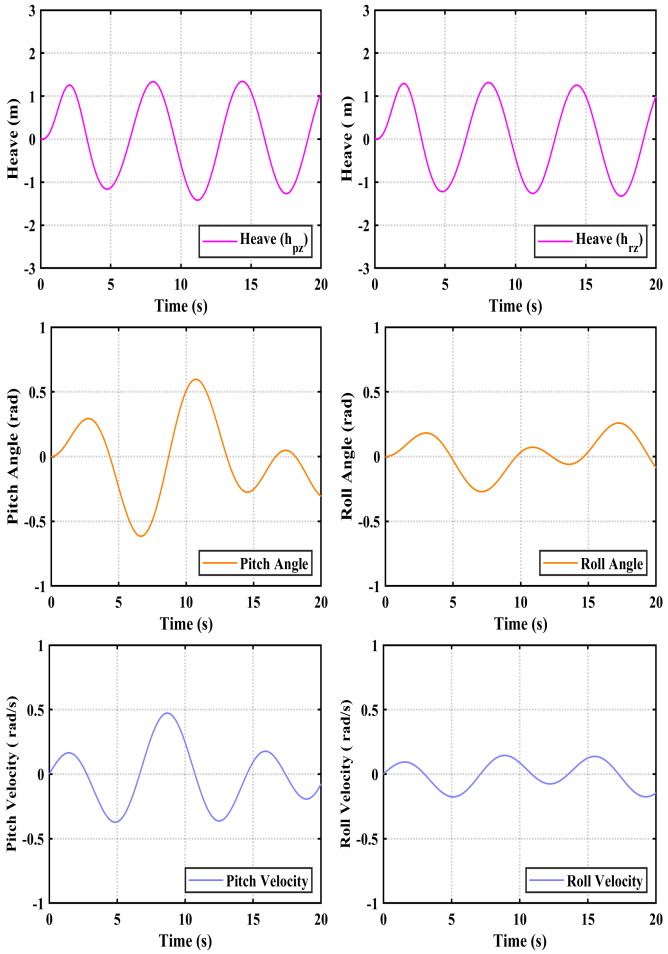

Fig. 4: Model output of pitch and roll for regular wave inputs.

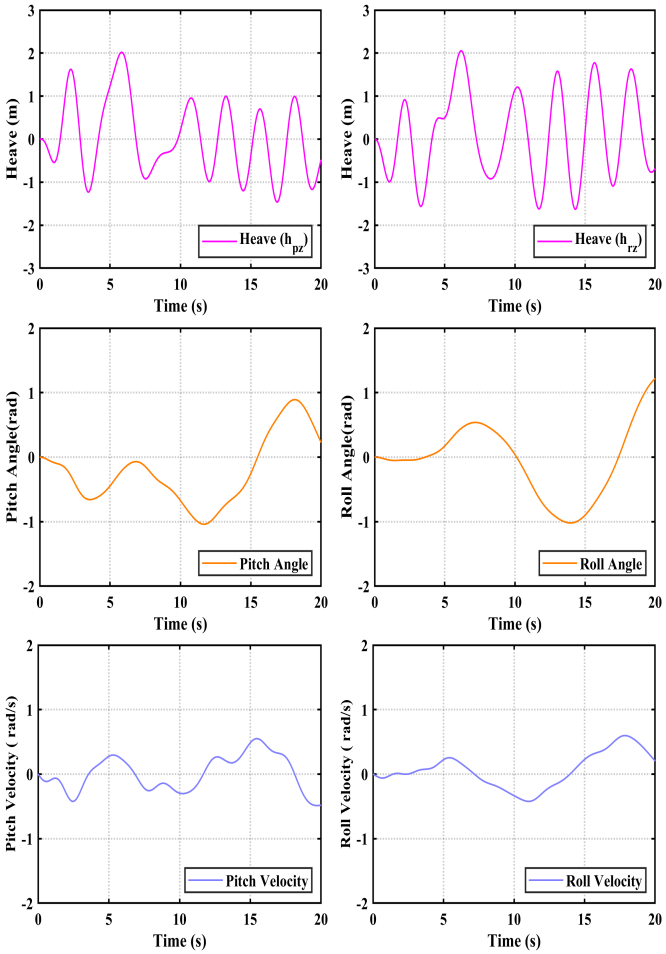

Fig. 5: Model output of pitch and roll for irregular wave inputs.

vehicle, and the vehicle reacts with rotation and elevation. To determine the motion of the vehicle, parameters listed in Table II are used.

There are two common approximations in heave-induced force and moment inputs in the literature [17]. One is regular wave input, and the other is irregular wave input. The regular wave inputs are idealized waves characterized by constant amplitude, period, and wavelength. The regular wave model is commonly defined by a uniform sinusoidal force and moment. The irregular wave input aim to reflect the chaotic and random waves observed in real seas. They are described mathematically by spectral analysis or stochastic processes. In this study, regular and irregular wave inputs are used to derive the motion model. Two distinct inputs for roll and pitch are considered. For regular wave input, force and moment input are defined as

$$\begin{aligned} F_{p,r} &= 1 \times 10^{7} \sin(1.0t) \\ P_{p,r} &= 5 \times 10^{8} \cos(0.9t). \end{aligned} \tag{14}$$

For the irregular wave input, the spectral density function provides the force and moment input . Generally real sea wave data is used to define the spectral density function, and the spectral density function is converted to a time series. The time series is expressed as a sum of sinusoidal terms. Therefore, in this study, the sum of sinusoidal signals is used to determine the force and moment input of the irregular wave. Thus, the irregular wave inputs are defined as

$$\begin{aligned} F_{p,r} &= \sum_{i=1}^{N} AF_i \sin(\omega_i t + \phi_i) \\ P_{p,r} &= \sum_{i=1}^{N} AP_i \cos(\omega_i t + \phi_i). \end{aligned} \tag{15}$$

N denotes the number of sine components. AF_i and AP_i are amplitude arrays. Frequency and phase are represented by ω_i and ϕ_i , respectively. The phase is randomly assigned between 0 and 2π, and the frequency is defined in 50 regular steps between 0.1 rad/s and 3.5 rad/s. Both roll and pitch are subjected to the same regular and irregular inputs. Considering Table II and equation (14), the model output is shown in Fig. 4 for regular wave input. Both pitch and roll responses can be seen. Although sea waves are studied over a long periods, only a 20-second period is considered to determine the simulator's performance. In response to heave movement, the pitch and roll motions represent a combination of sinusoidal motion. So a lookup table can be implemented, and it can be easily integrated into the motion profile.

Based on Table II and equation (15), the model output for irregular wave input is illustrated in Fig. 5. Both pitch and

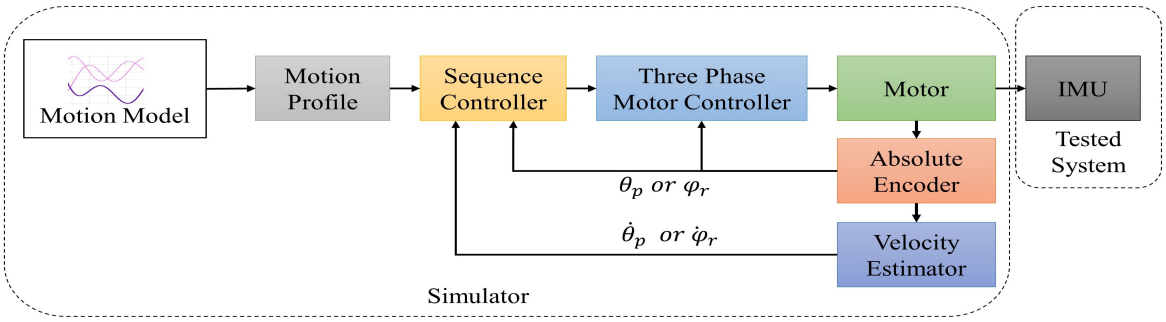

Fig. 6: Simulator control blocks.

roll responses are shown. The motion profile is produced for a 20-second interval. Compared to regular wave responses, pitch and roll responses form more complex shapes, but they can still be converted into a lookup table and applied to the simulator.

V. Sequence Controller

Tracking a motion profile creates a time-scheduling problem [18]. The best way to solve this problem is to use an algorithm. However, effective performance of the algorithm requires efficient time management. Fig. 6 shows the proposed control structure for the simulator. The motion profile transmits position and speed information to the controller. Position and speed steps are arranged for motion tracking. An algorithmic sequence controller generates the motor control input. The three-phase motor driver performs the motor's movements

The key point is to reach each step on time. The actuator of the simulator must be able to follow the steps. The movement caused by the interaction between marine vehicles and waves occurs at low frequencies. With an actuator that operates at relatively high frequencies, motion tracking becomes easier. However, the movements resulting from the interaction are nonlinear. Therefore, the motion profile may include irregular acceleration and jerk. This situation needs to be taken into consideration. To this end, system identification is utilized. A model of the motor is obtained that is approximated as the second-order. To obtain the motor model, a sweep function is applied to the motor in open-loop.

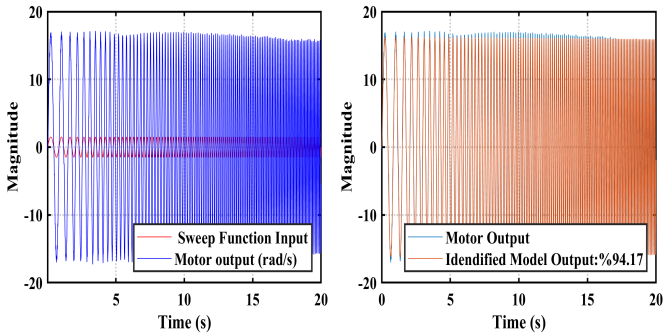

Fig. 7: Identification of motor model.

Fig. 7 shows the input response to the sweep function and the system identification result. The sweep function is implemented over a duration of 20 seconds, sweeping from 1 Hz to 10 Hz. System identification is applied to real-time data collected from the motor. The identified model is used to determine the control parameter variation. An approximate second-order motor transfer function is obtained as follows.

$$G(s) = \frac{1.1975 \times 10^6}{s^2 + 576.4353s + 1.1053 \times 10^5} \tag{16}$$

Although the PD controller can give a fast response in dynamic systems, its steady-state response is poor. It can also cause undesirable responses when parameters change. On the other hand, the steady-state response of the PI controller is strong. It is prone to parameter variations. However, its fast response requires effective adjustment of the refresh time. It also requires avoiding integral windup. In this study, the PI controller is preferred over the PD controller in motion profile tracking. For the PI controller, a high refresh rate is applied by taking advantage of the high speed of the microcontroller and the fast response of the brushless motor. The algorithm is used to avoid windup. Additionally, a parameter update algorithm is developed to ensure that the PI controller reaches each motion profile step on time.

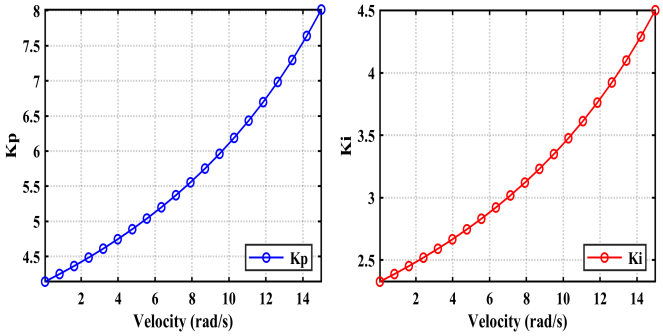

Fig. 8: Variation of Kp and Ki according to velocity.

The sequence controller includes an internal PI controller to track the target step. The parameters of the PI controller are updated based on the difference between the current position and the target position. This update is based on the motor velocity. The velocity range is defined between 0.05 and 15 rad/s. Assuming that the system's gain increases with speed, PI parameter variation is determined from the identified motor model. The pidtune function in MATLAB is used to determine

PI parameters. Fig. 8 shows the variation of the Kp and Ki parameters with respect to the velocity.

The motor's complementary sensitivity response is shown in Fig. 9. The PI controller parameters at three speed points are used for complementary sensitivity. It shows that the motor's tracking capability has a wide frequency range.The bandwidth is around 100 Hz. In this case, a high refresh rate is required so that changes in the PI parameters do not degrade the tracking performance.

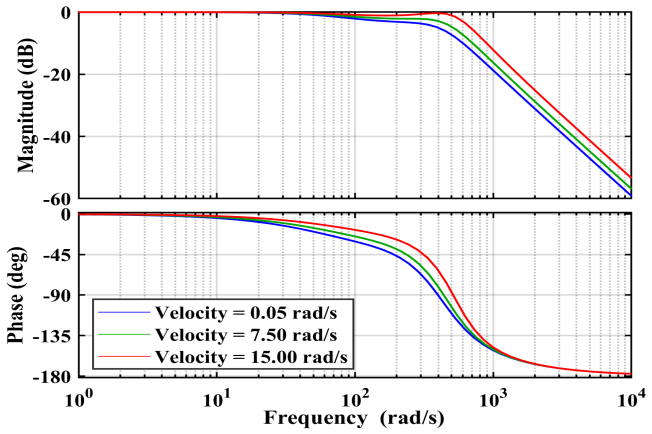

Fig. 9: Complementary sensitivity responses for velocities of 0.05 rad/s, 7.5 rad/s and 15 rad/s.

The sequence control algorithm first generates a target position lookup table using the motion profile. Each lookup table step is arranged at a 10 ms interval. Thus, the lookup table can be tracked at 100 Hz. The motor speed is adjusted by the internal PI controller to reach the target position. The sequence controller is run at 10 kHz. Thus, the internal PI controller runs at a refresh rate of 100 μs.

The algorithm of the sequence procedure is shown in Algorithm 1. The target step (tp) is updated when the current step (cp) is reached, and error integration is reset simultaneously. The target step change is subject to two conditions. The error falling below the specified value (sr_{th}) and the completion of the time set for the step (sq_{th}). The calculated control input (mc) is passed through a saturation filter and applied to the motor. The velocity (rps) is calculated for every ten cycles. This allows a 1 ms refresh rate for the velocity. The PI parameter update function is called every 1 ms .

The PI parameter update algorithm is shown in Algorithm 2. The remaining time (T_s) is calculated using step interval (10 ms) and completed time ($apd * 0.0001$). The difference between current position and target position provides a slope that contains target velocity information. The error ($derror$) between the slope and the current velocity (rps) is used to update the PI parameter. A error threshold value v_{th} determines whether the control parameters will be updated. Considering Fig. 8, both Kp and Ki have 20 points. There are two arrays to define Kp and Ki variation. An interpolation function is used to determine the intermediate values of the parameters.

Since the motor model is approximated by the system identification, it is not possible to fully characterize the engine.

Algorithm 1 Sequence Controller

Initializing
$tps[N] \leftarrow$ generate N component target positions
$cs \leftarrow 0$ initialize current state index
$er_{th} \leftarrow 0.001$ define error threshold
$sq_{th} \leftarrow 100$ set sequence threshold
$int \leftarrow 0$ set integral variable
$tp \leftarrow 0$ set target position
$apd \leftarrow 0$ set inner time index
$rps \leftarrow 0$ set velocity variable (radian per second)
$prv\_cs \leftarrow 0$ set previous position variable
$TKp, TKi \leftarrow$ initial PI parameters
$mc \leftarrow 0$ motor input variable
Procedure SEQUENCECONTROLLER()
$cp \leftarrow$ ReadAbsoluteEncoder()
$tp \leftarrow tps[cs]$
$error = tp - cp$
if $error \leq er_{th}$ *and* $apd \geq sq_{th}$ **then**
  $cs \leftarrow cs + 1$
  $apd = 0$
  $int = 0$
end if
$int = int + error$
if $apd \ \% \ 10$ **then**
  $rps \leftarrow (cs - prv\_cs)/0.001$
  $TKp, TKi \leftarrow$ UPDATEPIPARAMETER(apd,cp,cs,rps)
end if
$mc \leftarrow TKp * error + TKi * int$
Constrained(mc)
SendMotorCommand(mc,cp)
$apd \leftarrow apd + 1$
if $cs \geq N - 1$ **then**
  $cs \leftarrow 0$
  $apd \leftarrow 0$
end if
End Procedure

Algorithm 2 Update PI parameter

Initializing
$Kp[\,], Ki[\,] \leftarrow$ initialize Kp and Ki arrays.
$T_s \leftarrow 0$ remaining time
$\mu_1, \mu_2 \leftarrow$ set tune variables
$derror \leftarrow 0$ velocity error variable
$v_{th} \leftarrow$ set velocity threshold
Procedure UPDATEPIPARAMETER(apd,cp,cs,rps)
$T_s \leftarrow (0.01 - apd * 0.0001)$
$slope \leftarrow (tps[cs] - cp)/T_s$
$derror \leftarrow (slope - rps)$
if $|derror| \leq v_{th}$ **then**
  return TKp, TKi
else
  $TKp, TKi \leftarrow Interpolate(slope, Kp[\,], Ki[\,])$
  return $\mu_1 * TKp, \mu_2 * TKi$
end if
End Procedure

Therefore, additional parameters μ_1 and μ_2 are used to tune the variable Kp and Ki, respectively. The values of μ_1 and μ_2 are manually determined by observing the motor behavior.

VI. Experiments and Results

The motion models derived in Section IV are applied to analyze the performance of the simulator. Firstly, motion profiles generated with regular wave inputs are applied for pitch and roll. The simulator's outputs are shown in Fig. 10.

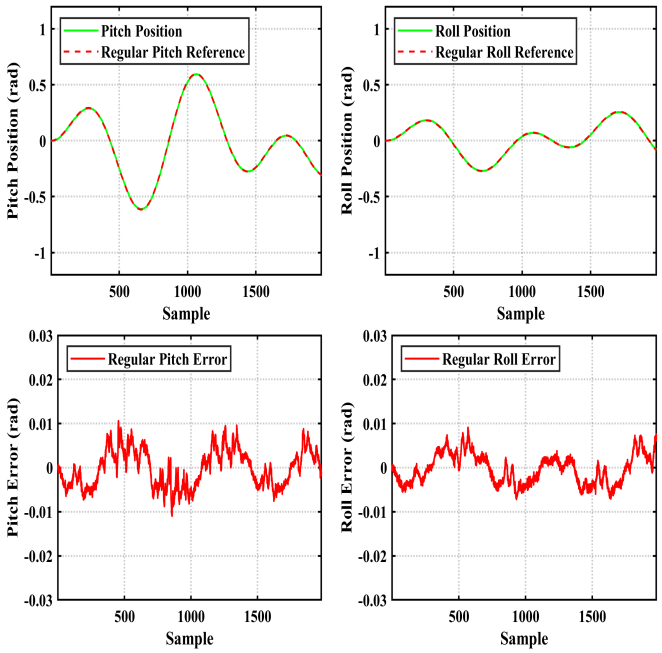

Fig. 10: Tracking response of pitch and roll under regular wave inputs.

In the first two figures, the red dashed line shows the reference, while the green line shows the simulator output. As seen, the motion profile can be tracked quite satisfactorily. The last two figures show the error between the simulator output and the reference. Secondly, the motion profiles generated with irregular wave inputs for pitch and roll are applied. The reference inputs and the simulator's outputs are shown in Fig. 11. As expected, tracking occurs within the irregular-wave motion profiles.

TABLE III: Tracking Performance

	Regular		Irregular	
	Pitch	Roll	Pitch	Roll
MAE	0.0036	0.0029	0.0038	0.0037
MAXE	0.0110	0.0091	0.0112	0.0118
RMSE	0.0042	0.0034	0.0044	0.0043

Error responses is used for performance analysis. The responses obtained as the ensemble average of outputs from 50 repeated experiments are evaluated. Three performance analyses are performed. Table III lists the performance results. The mean absolute error (MAE) indicates the overall performance of the simulator. When examined for each movement profile, It

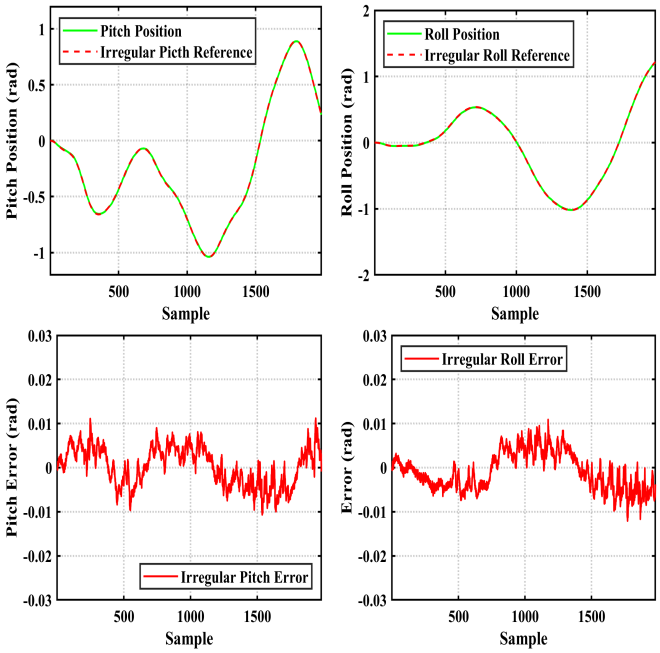

Fig. 11: Tracking response of pitch and roll under irregular wave inputs.

is seen that the maximum MAE is 0.0038. This indicates that the proposed simulator exhibits remarkable tracking performance. Another performance metric is the absolute maximum error (MAXE). It is observed that the MAXE value is less than 0.012 radians in all motion profiles. This highlights how accurately the simulator performs its analysis. The final metric is the Root Mean Square Error (RMSE). This metric also shows the simulator's tracking performance, similar to MAE. It is seen that the highest RMSE value is 0.0044. Therefore, the simulator demonstrates effective motion tracking capability.

In this study, the test system is the IMU. It is used to demonstrate the sensor responses. The simulator generates motion on a single axis. Therefore, to excite roll and pitch sensors, the IMU's position is changed. Fig.12 shows response of the IMU. The outputs of the y-axis gyroscope sensor and the x and z-axes accelerometer sensors can be seen for the pitch motion. The outputs of the x-axis gyroscope sensor and the x and z-axes accelerometer sensors can be seen for the roll motion.

The aim of this study is to design an effective, cost-effective, and compact simulator. The simulator can be used for sensor calibration, filter design, and algorithm analysis for marine navigation systems. Therefore, IMU sensor responses are shown as raw data without processing. When Fig. 12 is examined, it is observed that the accelerometers respond appropriately to the motion profile. On the other hand, the gyroscope exhibits inconsistent responses. The lowest selectable measurement range for the gyroscope sensor is 250 $^\circ/s$. Therefore, it may not respond to slow cyclic movements. This situation can be solved with a filtering method. For example, Kalman filter[19], Particle filter [20],etc. The proposed simulator can provide an analysis environment for the development of the filtering method.

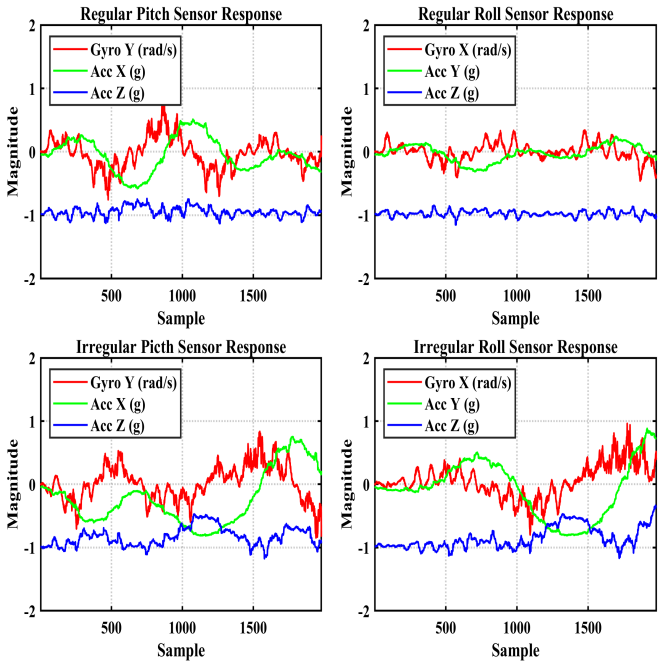

Fig. 12: Sensors outputs for regular and irregular wave inputs.

The proposed simulator structure can provide an effective test environment. However, especially in military applications, high-precision, often redundant, optical-based inertial sensors are used. These sensors have a wide measurement range and high sensitivity. In this case, it should be considered that the proposed simulator provides reference information with the encoder. On the other hand, the proposed algorithm can be applied to any motor-encoder system. Therefore, Accuracy of the simulator can be increased for high-precision inertial sensors with a high-precision motor-encoder system or external high precision position sensor.

VII. Conclusion

In this study, a hardware-based simulator is developed to investigate the effects of sea waves on ship navigation sensors. The aim is to develop a cost-effective, easy-to-implement, and effective simulator. Pitch and roll motion models resulting from the wave-heave relationship are taken into account. The mathematical models optained from the ship-wave interaction are used to generate the motion profile. Algorithmic sequence controller is developed to track the motion profile. A PI controller whose parameters can be updated is added within the sequence control. The performance of the simulator is demonstrated through experiments. Different motion profiles can also be applied to the simulator. The simulator consists of a single rotary actuator. The mechanical structure of the simulator is simpler compared to Stewart platforms and turntables. Therefore, the error impact due to the mechanical structure of the simulator is minimal. The portable size of the simulator allows for on-site testing and analysis. Additionally, the algorithm can be implemented on any motor- encoder system, so it is possible to analyze a bulky navigation sensor system with a powerful motor.

References

[1] A. M. Hasan, K. Samsudin, A. R. Ramli, R. S. Azmir, and S. A. Ismaeel, "A review of navigation systems (integration and algorithms)," *Australian Journal of Basic and Applied Sciences*, vol. 3, no. 2, pp. 943–959, 2009, available at: Universiti Putra Malaysia, Department of Computer and Communication System Engineering.

[2] Y. Kerwei, Y. Tsunlirng, and Z. Yujie, "A case study of yacht's motions represented by using stewart platform," in *Proceedings of the 27th Chinese Control Conference*, Chinese Automatic Control Society. Kunming, Yunnan, China: IEEE, July 2008, pp. 629–634.

[3] C. Han, X. Hu, and D. Sun, "The influence of ship roll and pitch on absolute measurement of ship heave signals and its correction method," *Ocean Engineering*, vol. 322, p. 120468, 2025.

[4] M. Richter, S. Schaut, D. Walser, K. Schneider, and O. Sawodny, "Experimental validation of an active heave compensation system: Estimation, prediction and control," *Control Engineering Practice*, vol. 66, pp. 1–12, 2017.

[5] J. Linder, M. Enqvist, and F. Gustafsson, "A closed-loop instrumental variable approach to mass and center of mass estimation using imu data," in *53rd IEEE Conference on Decision and Control*, 2014, pp. 283–289.

[6] L. F. M. V. Moraes, F. N. Carvalho, and H. P. P. Pereira, "Characterization and wave motion simulations of mems inertial sensors using 6dof platform," in *OCEANS 2019 - Marseille*, 2019, pp. 1–4.

[7] K. Talke, D. Drotman, N. Stroumtsos, M. de Oliveira, and T. Bewley, "Design and parameter optimization of a 3-psr parallel mechanism for replicating wave and boat motion," in *2019 International Conference on Robotics and Automation (ICRA)*, 2019, pp. 7955–7961.

[8] H. Yongpan and T. Limin, "Real-time zero phase filtering for heave measurement," in *2013 IEEE 11th International Conference on Electronic Measurement & Instruments*, vol. 1, 2013, pp. 321–326.

[9] E. Trinklein and G. Parker, "Ship motion sensor isolation system development and testing for use with low cost imus," in *2016 IEEE Sensors Applications Symposium (SAS)*, 2016, pp. 1–6.

[10] X. Liu, X. Xu, Y. Liu, and L. Wang, "A fast and high-accuracy transfer alignment method between m/s ins for ship based on iterative calculation," *Measurement*, vol. 51, pp. 297–309, 2014.

[11] X. Lu, C. Feng, Y. Ma, F. Yang, B. Shi, and D. Su, "Calibration method of rotation and displacement systematic errors for ship-borne mobile surveying systems," *Survey Review*, vol. 51, no. 364, pp. 78–86, 2019.

[12] T. Szelangiewicz, K. Żelazny, A. Antosik, and M. Szelangiewicz, "Application of measurement sensors and navigation devices in experimental research of the computer system for the control of an unmanned ship model," *Sensors*, vol. 21, no. 4, p. 1312, 2021.

[13] Y. Ma, Z. Yin, S. Wang, and Z. Chen, "Ship heave measurement method based on sliding adaptive delay-free complementary band-pass filter," *Ocean Engineering*, vol. 316, p. 119813, 2025.

[14] L. Wang, S. Li, J. Liu, Y. Hu, and Q. Wu, "Design and implementation of a testing platform for ship control: A case study on the optimal switching controller for ship motion," *Advances in Engineering Software*, vol. 178, p. 103427, 2023.

[15] A. Lloyd, *Seakeeping: Ship Behaviour in Rough Weather*, ser. Ellis Horwood Series in Polymer Science and Technology. E. Horwood, 1989. [Online]. Available: https://books.google.com.tr/books?id=LWwZAQAAIAAJ

[16] Y. Dai, R. Cheng, X. Yao, and L. Liu, "Hydrodynamic coefficients identification of pitch and heave using multi-objective evolutionary algorithm," *Ocean Engineering*, vol. 171, pp. 33–48, 2019.

[17] Y. ying Wang, "The specialist committee on waves final report and recommendations to the 23 rd ittc," 2016. [Online]. Available: https://api.semanticscholar.org/CorpusID:197643551

[18] H. Mu and Y. Zhou, "Profile generation algorithm and implementation for high accuracy motion," in *2006 IEEE International Conference on Robotics and Biomimetics*, 2006, pp. 549–554.

[19] K. Papafotis, G. Georgousis, C. Oustoglou, C. Dimas, and P. P. Sotiriadis, "A low-cost inertial measurement unit for ship motion estimation," in *2024 Panhellenic Conference on Electronics and Telecommunications (PACET)*, 2024, pp. 1–4.

[20] Y. Chen, X. Yang, and R. Liu, "A nonlinear sate estimate for dynamic positioning based on improved particle filter," in *2018 2nd IEEE Advanced Information Management,Communicates,Electronic and Automation Control Conference (IMCEC)*, 2018, pp. 880–884.

Ufuk GÜNER received the BS degree in 2005. He worked as a R&D engineer for more than eight years. He received the M.S. degree in Electrical Electronic Engineering from Ankara Yıldırım Beyazıt University in 2016 and the Ph.D. degree in Control and Automation Engineering from Yildiz Technical University in 2023. Since 2023, he has been an Assistant Professor with the Department of Electrical Electronic Engineering at Erzurum Technical University. His research interests include sensors, robotics, and control systems.